RSC Advances

PAPER

View Article Online
View Journal | View Issue

Cite this: *RSC Adv.*, 2024, **14**, 16982

Synthesis and spectral characterization of the phenothiazine-thiosemicarbazide probe for the optical solid-state detection of Hg^{2+} and Cu^{2+}†

Fatimah A. M. Al-Zahrani [a] and Mohamed A. Abdel-Lateef *[b]

Received 18th December 2023
Accepted 13th May 2024

DOI: 10.1039/d3ra08624k

rsc.li/rsc-advances

In this study, a phenothiazine-thiosemicarbazide (PTZDS) probe was synthesized and characterized. The synthesized PTZDS probe exhibited a yellow color, with a native fluorescence emission at $\lambda_{emission}$ = 550 nm and $\lambda_{excitation}$ = 450 nm. Over other metal ions, the probe exhibited significant selectivity and sensitivity towards Hg^{2+} and Cu^{2+}. The probe showed fluorescence quenching along with a minor shift in the absorbance spectra from 400 to 450 nm and 430 nm in the presence of Hg^{2+} and Cu^{2+}, respectively. In addition, the color of the synthesized probe remarkedly faded with the addition of Hg^{2+} or Cu^{2+}. Fluorescence measurements, infrared spectroscopy (IR), and density functional theory studies were employed to elucidate the binding process in the PTZDS + Cu^{2+} and PTZDS + Hg^{2+} sensor systems. Furthermore, photophysical investigations of the synthesized probe with Hg^{2+} and Cu^{2+} were performed. Finally, the probe was successfully employed as a solid-state thin layer chromatography (TLC) optical sensor for detecting Hg^{2+} and Cu^{2+} ions.

1. Introduction

Heavy metals are natural metallic elements that are toxic or harmful when absorbed even in small doses and have a relatively high density.[1] In their natural form, heavy metals can also be found in the crust of Earth. They occasionally enter human bodies through the air, food, and water. As trace elements, some heavy metals such as zinc, selenium, and copper are essential and required at very low concentrations for regulating body metabolism.[2,3] However, they become toxic when their concentrations exceed specific thresholds.[4] The bioaccumulation potential of heavy metals gives rise to significant concerns. Heavy metal contamination of water resources can originate from numerous sources including consumer and industrial waste, weathering of rocks, volcanic eruptions, and acid rain, which decompose the soil and release metals into streams, rivers, lakes, and groundwater.[5–7] One of the frequently used heavy metals is copper (Cu). It is typically used in electronic chips, water pipes, batteries, mobile phones, semiconductors, pulp and paper industry, fungicide and pesticide industries, and manufacturing catalysts and products for metal processing.[8–11] Although Cu is essential for proper growth of living things, high doses of copper may be quite dangerous. In high doses, copper is poisonous and can lead to nausea, diarrhea, weakness, or, in cases of severe exposure, liver cirrhosis. Similar to iron (Fe), copper may take part in chemical processes that generate highly reactive oxygen species (ROS), which are in charge of lipid oxidation in membranes, direct oxidation of proteins, and breaking of RNA and DNA strands.[12,13] Aging and numerous illnesses including disorders of the neurological system and cancer are largely influenced by the production and activation of ROS.[14] Cu toxicity may also occur with the displacement of other metal co-factors from their native ligands, in addition to the production of ROS. For example, the human estrogen receptor changes its signal transmission function *in vivo* when Cu(II) enters the zinc-finger DNA binding domain and replaces Zn(II).[15] To stop the buildup of Cu ions to dangerous levels, specific regulatory mechanisms should be established.

Mercury is a hazardous, bioaccumulative, and persistent contaminant.[16–18] It is classified as the third most dangerous metal by the US Government Agency for Dangerous Substances and Disease Registry, after lead and arsenic.[19,20] Environmental mercury exists in three forms: inorganic mercuric (Hg^{2+}), metallic mercury, and mercurius salts and organic molecules (such as methyl-, ethyl-, and phenyl-mercury). Although all forms of mercury are dangerous, their toxicokinetic profiles vary, with organic mercury being the most toxic and elemental the least. Inorganic mercury salts, such as inorganic mercurous (Hg) and mercuric (Hg^{2+}), are composed of inorganic mercury plus one of the following three elements: oxygen, chlorine, or sulfur. Mercury is also released into the atmosphere from

[a]*Chemistry Department, Faculty of Science, King Khalid University, PO Box 9004, Abha 61413, Saudi Arabia*

[b]*Department of Pharmaceutical Analytical Chemistry, Faculty of Pharmacy, Al-Azhar University, Assiut Branch, Assiut 71524, Egypt. E-mail: mohamed_abdellateef@azhar.edu.eg*

† Electronic supplementary information (ESI) available. See DOI: https://doi.org/10.1039/d3ra08624k

a variety of anthropogenic and natural sources, including (i) primary natural sources, such as volcanic eruptions, rock weathering, geothermal activity, and soil erosion, which account for 10% of emissions; (ii) primary anthropogenic sources, which include mining and extraction of fossil fuels like coal, gas or oil; (iii) consequent anthropogenic sources like mercury-dependent small-scale gold mining [ASGM], various manufacturing procedures across the chloralkaline industry, which account for 30%; and (iv) re-utilisation and re-radiation (biomass blazing, forest exculpating, wildfires), which represent 60%. Anthropogenic activities have nearly quadrupled the quantity of mercury in the atmosphere and are responsible for the annual increase in atmospheric load by 1.5 percent. As a consequence of expanding industrial, medical, and home use, mercury concentrations are continually rising, creating a global concern. Mercury thresholds of 0.01 mg L^{-1} for industrial effluents and 0.001 mg L^{-1} for drinking water were established by the Bureau of Indian Standards and the WHO.[21,22] Mercury poisoning has a severe impact on the neurological system as it can interfere with energy generation, disrupting cellular detoxification processes and forcing the cell to either die or exist in a chronically malnourished condition.[23,24]

As a result, scientists working in a variety of sectors are developing novel, accurate, and quick ways to detect these heavy metals. Due to their excellent sensitivity, selectivity, and low cost,[25–28] fluorescence sensors hold the potential to be one of the most effective heavy metal ion detection technologies.[25] Numerous fluorescent probes have recently been discovered for simultaneously detecting Cu^{2+} and Hg^{2+}.[29,30] A majority of Hg^{2+} chemosensors work by coupling Hg^{2+} with numerous N atoms or S atoms in well-known fluorophores, such as rhodamine, pyrene, coumarin,[31] or BODIPY derivatives.[32] A common method for developing novel fluorescent probes for Hg^{2+} is chemo dosimetry.

Using the phenothiazine (PTZ) core, which shows strong luminescence and excellent photo-responsivity and is often employed as an electron donor in dye-sensitized solar cells and organic light-emitted diodes,[33–36] for heavy metal detection is a novel strategy. To the best of our knowledge, there have been just a few reports on using fluorescent probes based on PTZ.[29,37,38] The creation of a PTZ fluorescence probe, namely the phenothiazine-thiosemicarbazide compound, for detecting Hg^{2+} ions and Cu^{2+} ions at nanomolar concentrations is described in this work. For Hg^{2+} ions and Cu^{2+} ions in aqueous solutions, this compound functions as a colorimetric and highly selective fluorescence probe.

2. Experimental methods

2.1 Materials and instruments

Solvents purchased from Sigma Aldrich were utilized without purification. The purity of the products was checked using

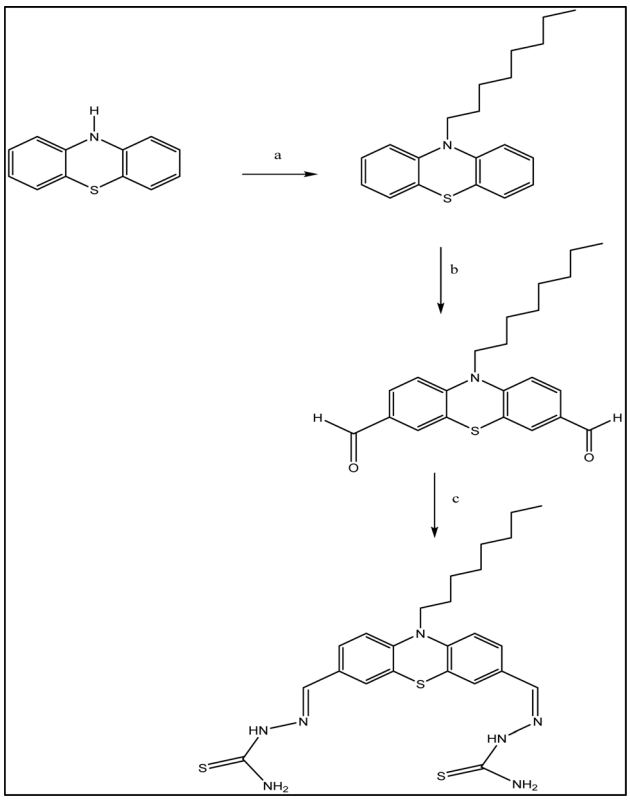

Scheme 1 Synthesis of PTZDS. (a) Mixing of DMSO and K_2CO_3 for 24 hours; (b) refluxing of DMF and $POCl_3$ for 24 hours; (c) stirring of thiosemicarbazide for 4 hours at room temperature in EtOH.

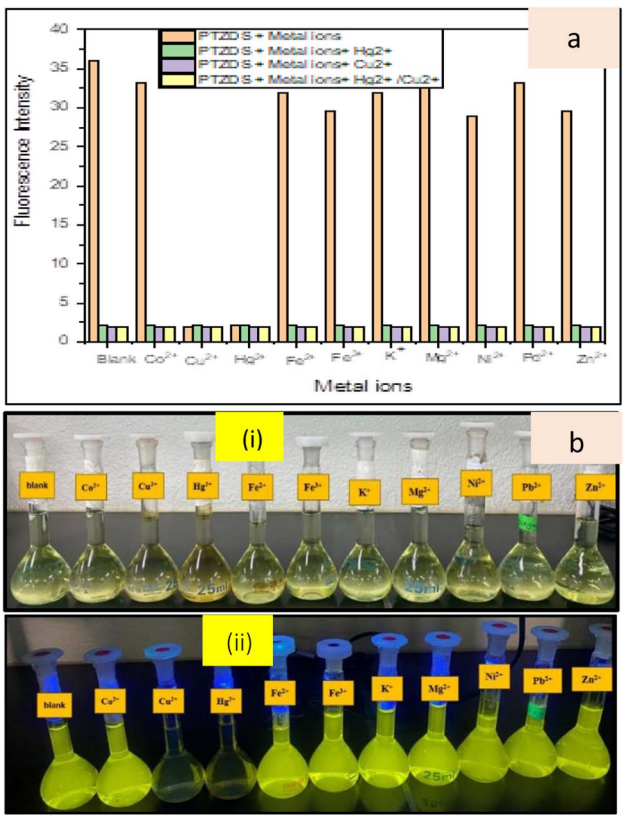

Fig. 1 (a) Selectivity and competitive binding of PTZDS towards Hg^{2+} and Cu^{2}, and (b) photos of PTZDS with different metal ions under (i) daylight and (ii) UV lighting.

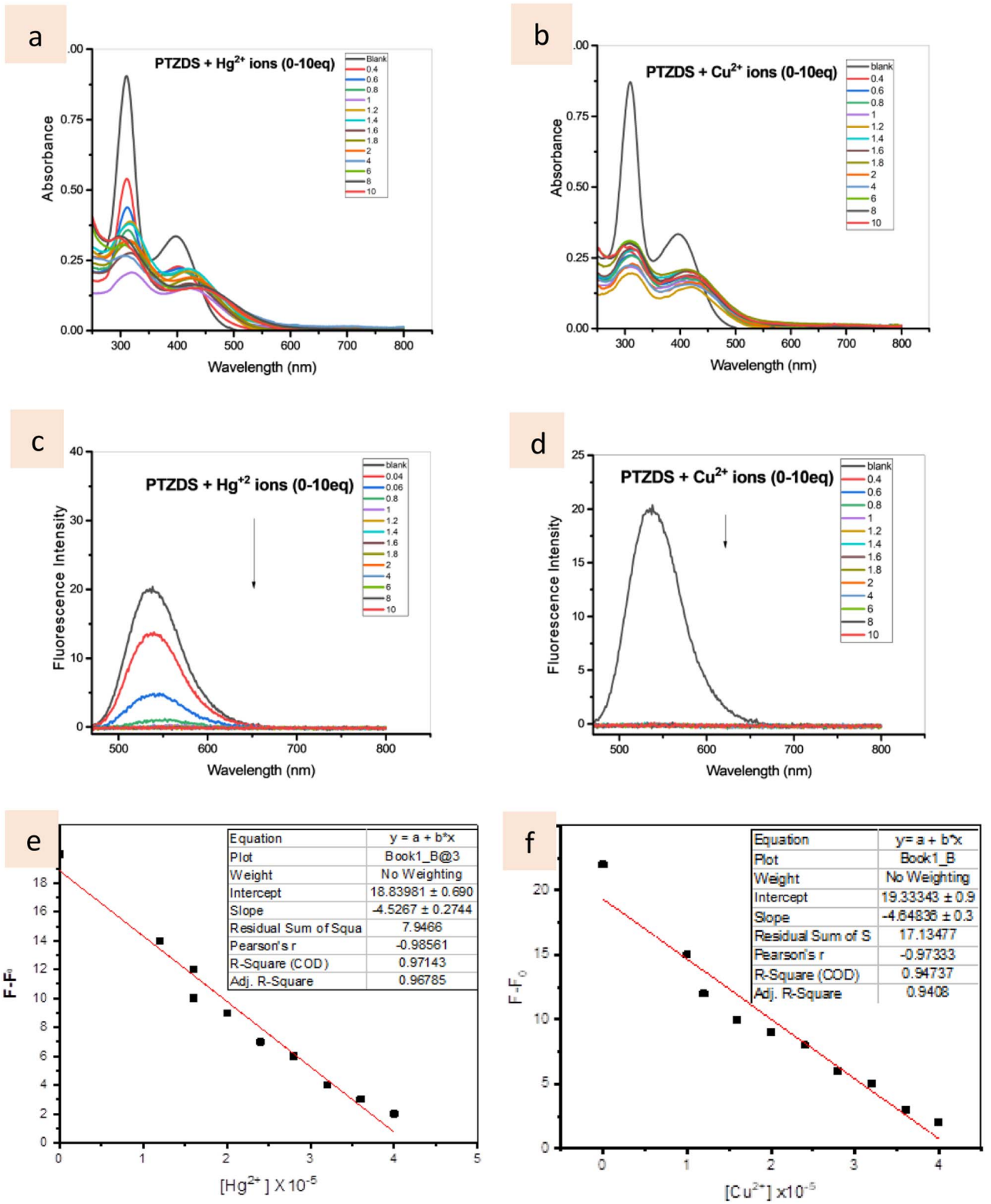

Fig. 2 (a and b) Changes in the absorption spectrum of the probe (10^{-5} M) with the addition of Hg^{2+} and Cu^{2+}, respectively; (c and d) fluorescence emission spectra of the probe (10^{-5} M) with the addition of Hg^{2+} and Cu^{2+}, respectively; (e) linear relationship between the fluorescence intensity of PTZDS and the concentration of Hg^{2+}; (f) linear relationship between the fluorescence intensity of PTZDS and the concentration of Cu^{2+}.

aluminum silica gel F_{254}-TLC, and any spots observed were identified based on the absorption of UV light. NMR spectra were captured in DMSO-d_6 using Bruker Avance 850 MHz and 213 MHz spectrometers. The chemical shifts (δ) are reported in ppm, and coupling constants are given in Hz. A UV-vis absorbance spectrophotometer (Agilent 8453) in the wavelength range of 250–800 nm was utilized to record the UV-vis absorbance spectra. A Hitachi F-7000 fluorescence spectrometer device was utilized to obtain the fluorescence spectra.

2.2 Synthetic procedures

2.2.1. Synthesis of the PTZDS probe. Twenty milliliters of ethanol were used to dissolve 1 mmol 10-octyl-10*H*-phenothiazine-3,7-dicarbaldehyde and 2 mmol thiosemicarbazide. The mixture was then stirred at room temperature for 4 hours. A large amount of water was added, and the solution was then filtered to obtain a yellow precipitate. After that, the obtained substance was purified by crystallization in ethanol to produce the probe (PTZDS) (90%), m.p.: 145 °C; ^{1}H NMR (850 MHz, DMSO-d_6); 0.799 (t, 3H, CH_3), 3.95 (t, 2H, CH_2–N),7.008 (d, 2H, $J = 8.5$ Hz, Ar–H), 7.494 (dd, 2H, $J = 8.5$,1.7 Hz, Ar–H), 7.700 (d, 2H, $J = 1.7$ Hz, Ar–H), 7.924 (s, 2H, Ar–H), 8.022 (s, 2H, NH_2), 8.130 (s, 2H, CH=N), 11.324 (s, 2H, NH). ^{13}C NMR (213 MHz, DMSO-d_6); 14.39, 22.46, 26.34, 26.42, 28.87, 29.01, 31.51, 47.26, 116.23, 116.35, 116.80, 123.60, 123.64, 123.84, 125.33, 128.25, 128.43, 129.29, 130.14, 141.40, 141.71, 144.54, 145.48, 178.06 and IR (cm^{-1}, KBr): 3425.89, 3258.88, 3147.86, 2922.45, 2851.39, 2360.96.

2.3. Solvent selection and metal detection

A variety of solvents were tested to determine the best "off-on" ratio. Selectivity toward Hg^{2+}/Cu^{2+} ions was better in acetonitrile than other solvents. Furthermore, we also performed PTZDS spectral titrations with various ratios (0–90% with an equal span of 10%) of H_2O for efficient selectivity. The probe demonstrated a greater "off-on" sensory response to Hg^{2+}/Cu^{2+} only in CH_3CN/H_2O (v/v, 1 : 1).

UV-visible and spectrofluorimetric titrations were conducted for the probe solution in CH_3CN/H_2O (v/v, 1 : 1) at a concentration of 10^{-5} M. A 10^{-4} M stock solution of the probe was prepared, and the metal ions used were Co^{2+}, K^+, Mg^{2+}, Ni^{2+}, Fe^{2+}, Fe^{3+}, Pb^{2+}, Zn^{2+}, Cu^{2+}, and Hg^{2+} (2×10^{-3}M). The UV spectra was measured between 250 and 800 nm, the fluorescence spectra were obtained after excitation at 450 nm, and the fluorescence emission was scanned and measured between 500 and 800 nm.

2.3.1. The limit of detection of PTZDS toward $Hg^{2+}$and Cu^{2+}. The equation below was utilized to determine the detection limit (LOD):

$$\mathrm{LOD} = 3S/\rho \quad (1)$$

where S is the slope of the intensity *versus* sample concentration curve, and ρ is the standard deviation of blank measurements (10 runs).

3. Results and discussion

3.1. Synthesis and characterization of PTZDS

10-Octyl-10*H*-phenothiazine-3-carbaldehyde (1) and thiosemicarbazide (2)[39] were used to synthesize the probe (PTZDS), as shown in Scheme 1. ^{1}H NMR, ^{13}C NMR, and IR were used to characterize PTZDS (Fig. S1 and S2 in ESI†).

3.2 Selectivity of PTZDS toward Hg^{2+} and Cu^{2+} *versus* other metal ions

PTZDS was evaluated against a number of important metal ions, including Co^{2+}, Pb^{2+}, Zn^{2+}, K^+, Mg^{2+}, Ni^{2+}, Fe^{2+}, Fe^{3+}, Cu^{2+}, and Hg^{2+}, in order to examine its selectivity towards Hg^{2+} and Cu^{2+}. The addition of the aforementioned metal ions had no discernible effect on the intensity of the fluorescence spectra of PTZDS (Fig. 1). In addition, the fluorescence behavior of various

Table 1 Limit of detection of the PTZDS sensor toward Cu^{2+}/Hg^{2+} in comparison with other reported sensors

Method	Analyte	Solvent	LOD, M
6 and 41	Cu^{2+} and Hg^{2+}	EtOH/H_2O (HEPES, pH 7.4) 4 : 1 (v/v)	1.63×10^{-6} (Cu) 2.36×10^{-6} (Hg)
42	Cu^{2+} and Hg^{2+}	EtOH/water (2 : 1, v/v) buffer (HEPES, pH 7.2)	3.37×10^{-6} (Cu) 1.50×10^{-7} (Hg)
43	Cu^{2+} and Hg^{2+}	MeCN	8.0×10^{-8} (Cu) 5.3×10^{-7} (Hg)
44	Cu^{2+} and Hg^{2+}	THF/HEPES buffer (8 : 2, v/v, pH 7.4)	9.7×10^{-8} (Cu) 8.0×10^{-8} (Hg)
45	Cu^{2+} and Hg^{2+}	MeCN/H_2O (7/3, v/v)	2.3×10^{-8} (Cu) 3.2×10^{-7} (Hg)
46	Cu^{2+} and Hg^{2+}	MeCN/HEPES (8 : 2, v/v, pH 7.4)	1.9×10^{-8} (Cu) 0.77×10^{-8} (Hg)
47	Cu^{2+} and Hg^{2+}	MeOH/H_2O (1 : 1, v/v)	3.6×10^{-7} (Cu) 2.49×10^{-6} (Hg)
The present work	Cu^{2+} and Hg^{2+}	CH_3CN/H_2O (v/v, 1 : 1)	8.0×10^{-9} 9.7×10^{-9}

metal ions in hindering the binding of Hg^{2+} and Cu^{2+} binding to PTZDS was investigated. A viable investigation showed that fluorescence quenching caused by Hg^{2+} and Cu^{2+} (1 equiv.) in the presence of other metal ions (1 equiv.) were equivalent to those in the presence of Hg^{2+} and Cu^{2+} alone (Fig. 1). These findings suggest that PTZDS is far more sensitive and selective to Hg^{2+} and Cu^{2+} than other competing metal ions. Fig. 1 shows the competitive binding and selectivity of PTZDS towards Hg^{2+} ions and Cu^{2+} ions. The green and purple bars show the fluorescence intensities of PTZDS + metal ions + Hg^{2+}, and PTZDS + metal ions + Cu^{2+}, respectively, while the yellow bars show the fluorescence intensity values of PTZDS in the presence of only Hg^{2+} and Cu^{2+}.

Table 2 Photophysical and DFT properties of PTZDS and its sensor complexes

Composition	Tot E[a]	HOMO (eV)	LUMO (eV)	HLG[b] (eV)	Φ
PTZDS	−2509.56	−5.34	−2.18	3.16	0.269
PTZDS + Hg^{2+}	−1387.63	−5.90	−2.97	2.93	0.033
PTZDS + Cu^{2+}	−4149.04	−4.53	−1.90	2.63	0.041

[a] Total energy. [b] HOMO–LUMO gap, quantum yields in $CH_3CN : H_2O$ (1/1) using 9,10-diphenylanthracene ($\Phi = 0.9$) as the reference.

3.3. Photophysical studies of PTZDS with Hg^{2+} and Cu^{2+}

Absorbance bands at 300 and 400 nm were observed for the PTZDS (10^{-5} M) solution in CH_3CN/H_2O (v/v, 1 : 1). The absorbance bands at 300 and 450 nm decreased with the addition of Hg^{2+} ions (0–10 equiv.), as seen in Fig. 2a and S3,† but the absorbance peak at 400 nm marginally increased (50 nm red-shift). Similar results were observed when the PTZDS solution was titrated with Cu^{2+} ions (0–10 equiv.) In Fig. 2b and S3,† a red-shifted band at can be seen at 450 nm. The stoichiometries of the complexes produced between PTZDS and the Hg^{2+} ions or Cu^{2+} ions were calculated using Job's plots as reported in a previous study.[40] These findings suggest a 1 : 1 stoichiometry for the binding of PTZDS to these metal ions.

In the CH_3CN/H_2O (v/v, 1 : 1) solution, PTZDS (10^{-5} M) was investigated for its fluorescence spectroscopic characteristics in

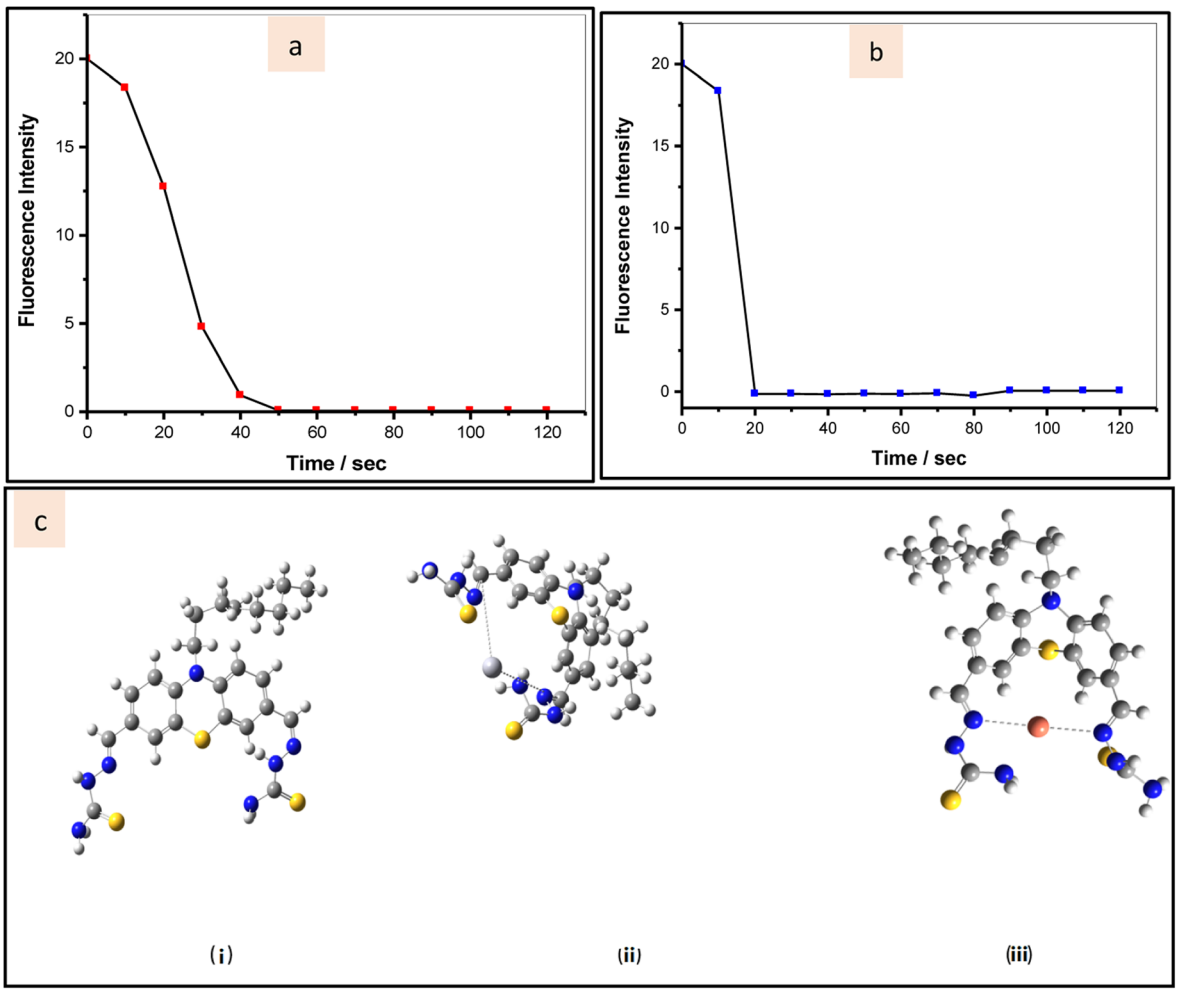

Fig. 3 (a and b) Variations in PTZDS fluorescence at 550 nm as a function of time in the presence of Hg^{2+} and Cu^{2+}, respectively; (c) optimized structures of the (i) PTZDS probe, (ii) PTZDS + Hg^{2+}, and (iii) PTZDS + Cu^{2+}.

the presence of Hg^{2+} ions and Cu^{2+} ions. PTZDS displayed an emission band at 550 nm after excitation at 450 nm (using slit widths of 5 nm for excitation and emission). Hg^{2+} treatment, however, caused the fluorescence signal at 550 nm to totally disappear (>80%) (Fig. 2c). A similar fluorescence quenching effect was seen at 550 nm (100%) after titrating the PTZDS solution with Cu^{2+} (0–10 equiv.) (Fig. 2d). Furthermore, the linear relationship between the fluorescence intensity and the concentrations of Hg^{2+} and Cu^{2+} are presented in Fig. 2e and f, respectively. According to these results, the detection limits (LOD) for Hg^{2+} ions and Cu^{2+} ions at 550 nm were calculated as 8.0×10^{-9} and 9.7×10^{-9} mol L^{-1}, respectively. The LOD values show that the as-prepared probe is sensitive enough to detect Hg^{2+} and Cu^{2+} quantitatively. Table 1 offers a comparison of the LOD of previously reported chemosensors with the PTZDS sensor, demonstrating that PTZDS is the most sensitive sensor reported thus far.

Radiative quantum yield (Φ) is a crucial parameter in molecular chemistry as it offers valuable insights into several aspects, such as excited electronic states, electronic-to-vibrational coupling, and radiationless transitions. By using eqn (2), the fluorescence quantum yield values (Φ) of PTZDS, PTZDS + Hg^{2+}, and PTZDS + Cu^{2+} in ethanol were calculated in comparison with the reference fluorescence quantum yield value of 9,10-diphenylanthracene.

$$\phi = \phi_R \frac{F}{F_R} \frac{\mathrm{OD}_R}{\mathrm{OD}} \frac{n^2}{n_R{}^2} \quad (2)$$

The subscript R indicates the reference fluorophore with a known quantum yield, n represents the refractive index, OD represents the optical density, and F represents the integrated fluorescence intensity. Table 2 displays the quantum yield values of PTZDS only, PTZDS + Hg^{2+}, and PTZDS + Cu^{2+}.

Further, we used time-dependent fluorescence responses to analyze the reaction kinetics of the utilized probe in presence of Hg^{2+} ions and Cu^{2+} ions. In the presence of Hg^{2+}, which encourages PTZDS hydration, the fluorescence intensity of PTZDS noticeably dropped after 40 seconds (Fig. 3a). Similar to this, the probe interaction with Cu^{2+} ended after 20 seconds (Fig. 3b).

3.4 DFT and FT-IR studies of PTZDS with Hg^{2+} ions and Cu^{2+} ions

As observed in Scheme 2, the formation of the PTZDS + Cu^{2+} and PTZDS + Hg^{2+}complexes were also well-supported by density

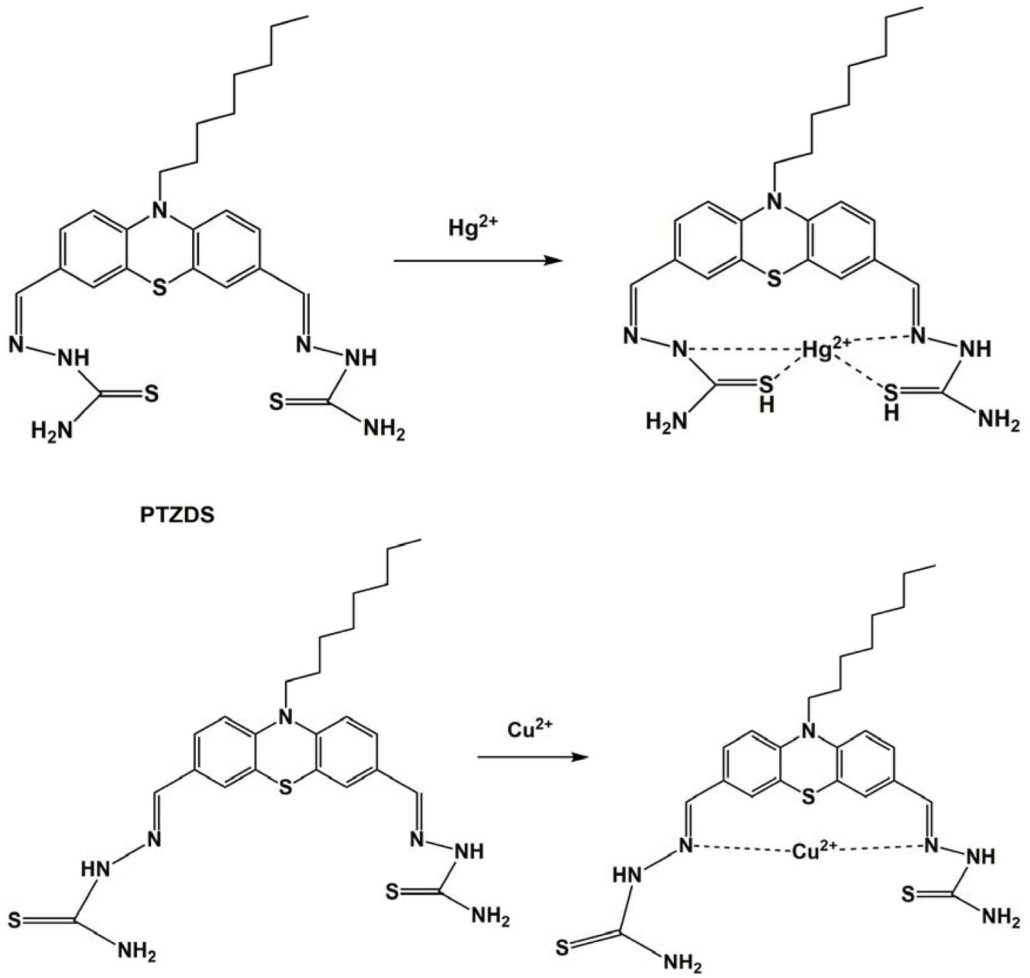

Scheme 2 Suggested mechanisms for the binding of PTZDS with Hg^{2+} and Cu^{2+}.

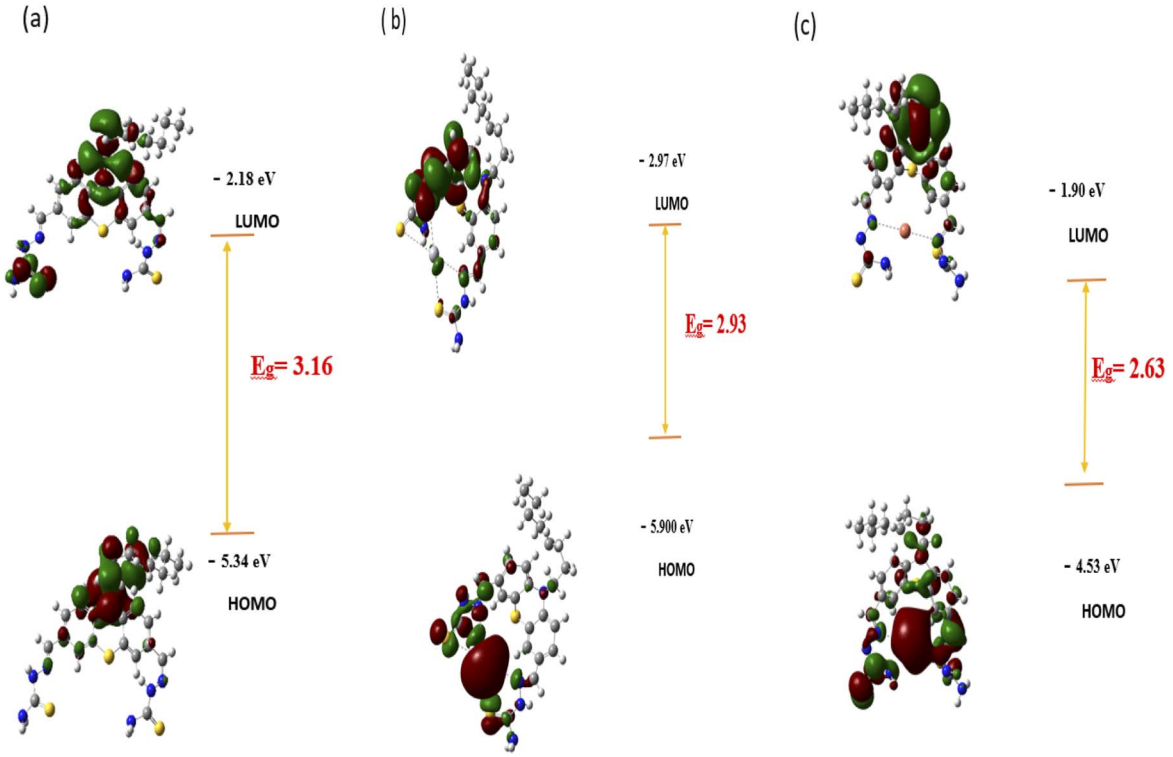

Fig. 4 HOMOs, LUMOs, and bandgaps of (a) PTZDS, (b) PTZDS + Hg^{2+} and (c) PTZDS + Cu^{2+}.

functional theory (DFT) studies. DFT calculations were performed using the Gaussian 09 software to clarify the structures of PTZDS, PTZDS + Cu^{2+}, and PTZDS + Hg^{2+}. By employing the B3LYP/6-31G basis set, B3LYP/LANL2DZ level energy optimization of the chemosensor PTZDS and the PTZDS + Hg^{2+}, and PTZDS + Cu^{2+} complexes was carried out. Fig. 3c displays the shapes of the used probe and the PTZDS + Hg^{2+} and PTZDS + Cu^{2+} complexes.

According to the DFT analysis, Hg^{2+} is situated between two S atoms at distances of approximately 2.1775 Å and 2.1600 Å. Similarly, Hg^{2+} is situated roughly 2.0400 Å and 2.0201 Å from the two N atoms. The HOMO–LUMO energy gaps discovered by DFT calculations, in particular, provided strong evidence for the excimer production mechanism. In addition, the bandgap of PTZDS was determined to be 3.16 eV between its HOMO (−5.34 eV) and LUMO (−2.18 eV). The bandgap between the HOMO (−5.90 eV) and LUMO (−2.97 eV), on the other hand, was further reduced to 2.93 eV as a result of the PTZDS + Hg^{2+} coordination. Table 1 lists the HOMO, LUMO, and energy gaps (HLP) calculated using DFT. Our additional analysis demonstrated that other than the bandgap, the electron density of PTZDS was dispersed across the structure, as shown in Fig. 4. This is attributable to the values obtained in DFT investigations. The electron transfer and emission intensity of PTZDS towards Hg^{2+} ions was affected, according to the aforementioned data. In order to detect Hg^{2+} ions, a fluorescent turn-off sensor response was therefore observed. According to these observations, the distances between the Cu atom and the two nitrogen atoms were 1.80 Å and 2.00 Å. In addition, the suggested mechanism for the coordination of Cu^{2+} and Hg^{2+} ions with the used probe *via* nitrogen agrees with other reported studies on the coordination of Hg^{2+} ions and Cu^{2+} ions with phenothiazine probes.[40,48]

FT-IR measurements were used to test the postulated process. By combining PTZDS with either $Cu(OCl_4)_2$ or $Hg(OCl_4)_2$ and potassium bromide, the IR spectra of PTZDS with Hg^{2+} and Cu^{2+} were captured (Fig. 5). The –NH stretching peak at 3425 cm^{-1} was shifted to 3586 cm^{-1}, and the C=N stretching band was shifted to 1613 cm^{-1} in the spectrum of PTZDS + Hg^{2+}. The peak of Hg–S=C was seen at 463 cm^{-1}. This indicated the binding of Hg^{2+} with the nitrogen and sulfur atoms. The Cu–N stretching signals of PTZDS -Cu(II) were first observed at 615 cm^{-1}.[49]

3.5 Application of PTZDS as a solid-state sensor

We examined the capacity of PTZDS to detect Hg^{2+} and Cu^{2+} on probe-pretreated TLC plates in order to determine the practical applicability of the solid-state sensor.[29] After a brief period of PTZDS (10^{-3} M) adsorption, the TLC plates were dried in the air. In the next step, the yellow TLC plates were treated with a solution of Hg^{2+} and Cu^{2+} (2 mL, 10^{-5} M) in water, and a sudden colour shift from yellow to dark was noticed for both Hg^{2+} and Cu^{2+}, as shown in Fig. 6. This experiment exhibits the solid-state Hg^{2+} and Cu^{2+} ion detection capability of PTZDS. This solid-state approach offers a straightforward, affordable, and practical alternative for the identification of Hg^{2+} ions and Cu^{2+} ions in environmental samples.

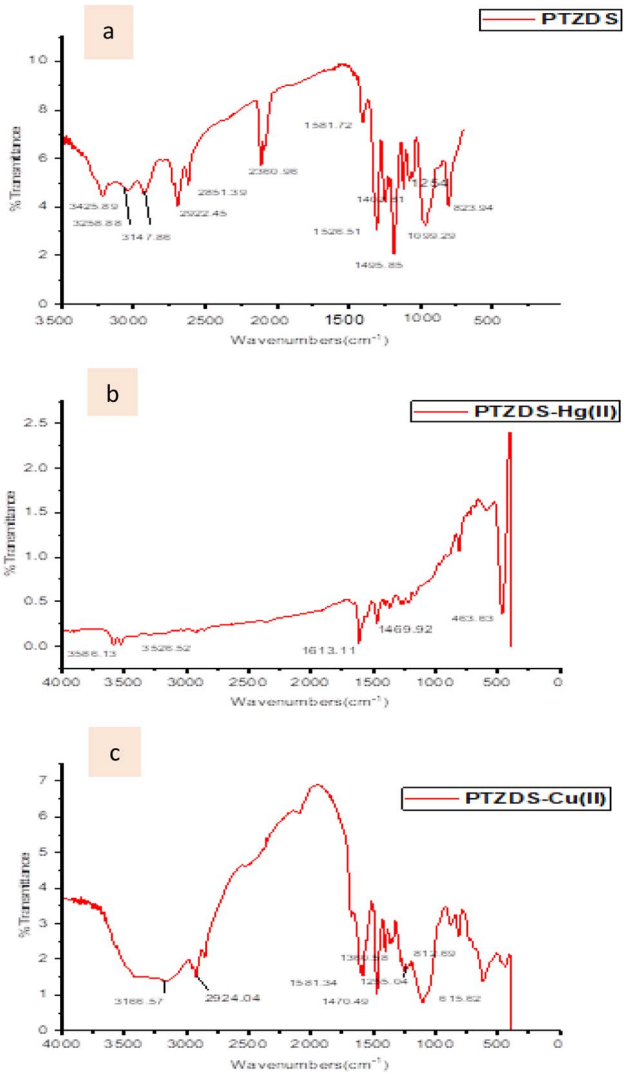

Fig. 5 IR spectra of (a) PTZDS, (b) PTZDS-Hg(II), and (c) PTZDS-Cu(II).

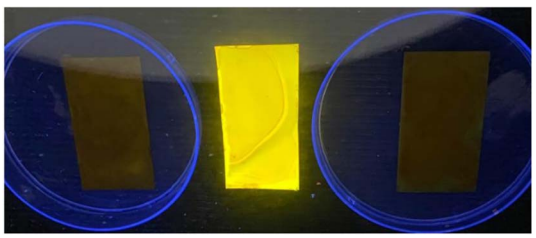

Fig. 6 Colour changes of PTZDS on TLC plates before and after the addition of Hg^{2+} and Cu^{2+}.

4. Conclusions

A colorimetric and fluorescent probe was synthesized based on phenothiazine-thiosemicarbazide. The synthesized probe was characterized by the ^{1}H NMR, ^{13}C NMR, and IR techniques. It exhibited a fluorescence emission at 550 nm after fluorescence excitation at 450 nm. The fluorescence intensity of the probe was remarkedly quenched upon the addition of either Hg^{2+} ions or Cu^{2+} ions. Moreover, the yellow color of the synthesized phenothiazine-thiosemicarbazide probe was also remarkedly quenched with the addition of Hg^{2+} or Cu^{2+} ions. The sensitivity and selectivity of the synthesized phenothiazine-thiosemicarbazide probe toward Hg^{2+} and Cu^{2+} were studied and found to be good. Furthermore, photophysical studies of the synthesized probe with Hg^{2+} and Cu^{2+} were performed. The interaction between the synthesized probe and Hg^{2+} and Cu^{2+} was studied and analyzed by density functional theory calculations and infrared spectroscopic analysis. Moreover, a solid-state optical sensor fabricated using the synthesized probe proved successful in detecting Hg^{2+} and Cu^{2+}.

Author contributions

Fatimah Al-Zahrani designed the research, carried out experiments, interpreted the results, resources, and methodology, supervised the data, and wrote and edited the main manuscript. Mohamed A. Abdel-Lateef writing – original draft and writing – review & editing.

Conflicts of interest

The authors declare no competing interests.

Acknowledgements

The authors extend their appreciation to the Deanship of Scientific Research at King Khalid University for funding this work through large group Research Project under grant number RGP2/143/44.

References

1 R. M. El-Shishtawy, M. M. Rahman, T. A. Sheikh, M. Nadeem Arshad, F. A. Al-Zahrani and A. M. Asiri, *Materials*, 2020, **13**, 2695.
2 F. A. Al-Zahrani, B. M. Al-Shehri and R. M. El-Shishtawy, *Sustainability*, 2023, **15**, 4700.
3 F. A. Al-Zahrani, B. M. Al-Shehri, R. M. El-Shishtawy, N. S. Awwad, K. A. Khan, M. Sayed and S. M. Siddeeg, *Materials*, 2022, **15**, 8136.
4 M. Jaishankar, T. Tseten, N. Anbalagan, B. B. Mathew and K. N. Beeregowda, *Interdiscip. Toxicol.*, 2014, **7**, 60.
5 B. M. Al-Shehri, F. A. Al-Zahrani, R. M. El-Shishtawy, N. S. Awwad, M. Sayed and K. A. Khan, *Sci. Rep.*, 2023, **13**, 1631.
6 X.-D. Jiang, J. Zhao, Q. Li, C.-L. Sun, J. Guan, G.-T. Sun and L.-J. Xiao, *Dyes Pigm.*, 2016, **125**, 136–141.
7 M. S. Sankhla, M. Kumari, M. Nandan, R. Kumar and P. Agrawal, *Int. J. Curr. Microbiol. Appl. Sci.*, 2016, **5**, 759–766.
8 F. A. Al-Zahrani, R. M. El-Shishtawy, A. M. Asiri, A. M. Al-Soliemy, K. A. Mellah, N. S. Ahmed and A. Jedidi, *BMC Chem.*, 2020, **14**, 1–11.
9 M. Parmar and L. S. Thakur, *Int. J. Plant, Anim. Environ. Sci.*, 2013, **3**, 143–157.

10 D. Kumar, H. Singh, A. Jain, V. Sharma, N. Bhardwaj, S. Puri and M. Khatri, *Chem. Pap.*, 2023, **77**, 1907–1920.
11 T. Simon, M. Shellaiah, V. Srinivasadesikan, C.-C. Lin, F.-H. Ko, K. W. Sun and M.-C. Lin, *New J. Chem.*, 2016, **40**, 6101–6108.
12 O. I. Aruoma, *J. Am. Oil Chem. Soc.*, 1998, **75**, 199–212.
13 C. Angelé-Martínez, K. V. T. Nguyen, F. S. Ameer, J. N. Anker and J. L. Brumaghim, *Nanotoxicology*, 2017, **11**, 278–288.
14 B. Halliwell and J. Gutteridge, *Biochem. J.*, 1984, **219**, 1.
15 P. F. Predki and B. Sarkar, *J. Biol. Chem.*, 1992, **267**, 5842–5846.
16 M. A. Abdel-Lateef, *Sci. Rep.*, 2022, **12**, 6953.
17 W. A. Al-Onazi and M. A. Abdel-Lateef, *Spectrochim. Acta, Part A*, 2022, **264**, 120258.
18 M. A. Abdel-Lateef, A. Almahri, E. Alzahrani, R. A. Pashameah, A. A. Abu-Hassan and M. A. El Hamd, *Chemosensors*, 2022, **10**, 358.
19 J. Wang, Q. Niu, T. Hu, T. Li and T. Wei, *J. Photochem. Photobiol., A*, 2019, **384**, 112036.
20 M. Shellaiah, Y. C. Rajan, P. Balu and A. Murugan, *New J. Chem.*, 2015, **39**, 2523–2531.
21 J. C. Clifton II, *Pediatr. Clin. North Am.*, 2007, **54**(2), e231–e245.
22 R. K. Verma, M. S. Sankhla and R. Kumar, *Int. J. Forensic Sci.*, 2018, **1**, 72–78.
23 A. Frustaci, N. Magnavita, C. Chimenti, M. Caldarulo, E. Sabbioni, R. Pietra, C. Cellini, G. F. Possati and A. Maseri, *J. Am. Coll. Cardiol.*, 1999, **33**, 1578–1583.
24 F. A. Al-Zahrani, H. A. Al-Ghamdi, M. A. Abdel-Lateef and R. M. El-Shishtawy, *Luminescence*, 2023, **38**, 477–486.
25 H. S. AlSalem, M. S. Binkadem, S. T. Al-Goul and M. A. Abdel-Lateef, *Spectrochim. Acta, Part A*, 2023, **295**, 122616.
26 M. A. Albalawi, H. Gomaa, M. A. El Hamd, M. A. Abourehab and M. A. Abdel-Lateef, *Luminescence*, 2023, **38**, 92–98.
27 M. S. Binkadem, H. S. AlSalem, S. T. Al-Goul, W. T. Alsaggaf, M. A. El Hamd and M. A. Abdel-Lateef, *Spectrochim. Acta, Part A*, 2023, **299**, 122839.
28 H. S. AlSalem, S. N. Alharbi, M. S. Binkadem, S. A. Mahmoud and M. A. Abdel-Lateef, *Luminescence*, 2024, **39**, e4748.
29 X. Lu, Y. Zhan and W. He, *J. Photochem. Photobiol., B*, 2022, 112528.
30 J. Hu, Z. Hu, Z. Chen, H.-W. Gao and K. Uvdal, *Anal. Chim. Acta*, 2016, **919**, 85–93.
31 S. O. Aderinto, *Chem. Pap.*, 2020, **74**, 3195–3232.
32 A. Roy, M. Nandi and P. Roy, *TrAC, Trends Anal. Chem.*, 2021, **138**, 116204.
33 L. M. Nhari, E. N. Bifari, A. R. Al-Marhabi, F. A. Al-Zahrani, H. A. Al-Ghamdi, S. N. Al-Ghamdi, A. M. Asiri and R. M. El-Shishtawy, *J. Organomet. Chem.*, 2023, **989**, 122648.
34 R. S. Rao, B. Yadagiri, G. D. Sharma and S. P. Singh, *Chem. Commun.*, 2019, **55**, 12535–12538.
35 F. AM Al-Zahrani, *Pigm. Resin Technol.*, 2022, 493–501.
36 A. Slodek, D. Zych, G. Szafraniec-Gorol, P. Gnida, M. Vasylieva and E. Schab-Balcerzak, *Materials*, 2020, **13**, 2292.
37 K. M. Vengaian, C. D. Britto, K. Sekar, G. Sivaraman and S. Singaravadivel, *Sens. Actuators, B*, 2016, **235**, 232–240.
38 P. Karuppusamy and S. Sarveswari, *Inorg. Chim. Acta*, 2021, **515**, 120073.
39 R. M. El-Shishtawy, F. A. Al-Zahrani, Z. M. Al-Amshany and A. M. Asiri, *Sens. Actuators, B*, 2017, **240**, 288–296.
40 V. Govindasamy, S. Perumal, I. Sekar, B. Madheswaran, S. Karuppannan and S. B. Kuppannan, *J. Fluoresc.*, 2021, **31**, 667–674.
41 M. Li, Y. Sun, L. Dong, Q.-C. Feng, H. Xu, S.-Q. Zang and T. C. Mak, *Sens. Actuators, B*, 2016, **226**, 332–341.
42 M. Ozdemir, *J. Photochem. Photobiol., A*, 2016, **318**, 7–13.
43 X. He, J. Zhang, X. Liu, L. Dong, D. Li, H. Qiu and S. Yin, *Sens. Actuators, B*, 2014, **192**, 29–35.
44 M. Kaur, M. J. Cho and D. H. Choi, *Dyes Pigm.*, 2016, **125**, 1–7.
45 D. Udhayakumari and S. Velmathi, *Supramol. Chem.*, 2015, **27**, 539–544.
46 D. Udhayakumari and S. Velmathi, *Ind. Eng. Chem. Res.*, 2015, **54**, 3541–3547.
47 Y. B. Wagh, A. Kuwar, S. K. Sahoo, J. Gallucci and D. S. Dalal, *RSC Adv.*, 2015, **5**, 45528–45534.
48 J. Wang, Q. Niu, T. Wei, T. Li, T. Hu, J. Chen, X. Qin, Q. Yang and L. Yang, *Microchem. J.*, 2020, **157**, 104990.
49 D. Vashisht, S. Sharma, R. Kumar, V. Saini, V. Saini, A. Ibhadon, S. C. Sahoo, S. Sharma, S. K. Mehta and R. Kataria, *Microchem. J.*, 2020, **155**, 104705.